STAR recent results on heavy ion collisions.

A. Aparin[a] *for the STAR collaboration* [1],

[a] Joint Institute for Nuclear Research, 6 Joliot-Curie St. Dubna, Moscow Region, Russia, 141980

Исследование плотной ядерной материи, образующейся в столкновениях тяжелых ионов, является одной из основных задач современной релятивистской ядерной физики. Релятивистский коллайдер тяжелых ионов (RHIC) предоставляет уникальную возможность исследовать фазовую диаграмму КХД, сталкивая различные типы ядер, а также изменяя энергию столкновений. На RHIC начался второй этап программы энергетического сканирования, в котором столкновения ядер золота будут происходить при энергиях $\sqrt{s_{NN}} = 7.7 - 27$ ГэВ. Набор данных в моде с фиксированной мишенью (FXT) позволит расширить доступный для анализа энергетический диапазон до $\sqrt{s_{NN}} = 3.0$ ГэВ. Набор данных в упомянутых программах значительно расширит наше представление о структуре фазовой диаграммы КХД в широком диапазоне бариохимического потенциала μ_B до 720 МэВ.

Недавние улучшения детекторов увеличили возможности STAR по регистрации частиц в области малых поперечных импульсов и больших псевдобыстрот, а также улучшили возможности по идентификации частиц. С новыми детекторами STAR значительно увеличивает точность вычислений, что может позволить исследовать как границу фазового перехода, так и образование “файербола”.

В этом докладе представлены свежие результаты и планы по дальнейшей работе эксперимента STAR.

Exploration of the hot and dense nuclear matter produced in collisions of heavy ions is one of the main goals of modern high energy nuclear physics. The Relativistic Heavy Ion Collider (RHIC) provides a unique opportunity to map the QCD phase diagram by colliding different nucleus species and varying the energy of collisions. RHIC has already begun the second phase of the Beam Energy Scan (BES) program, which will allow us to cover energy range for gold-gold collisions $\sqrt{s_{NN}} = 7.7 - 27$ GeV. The Fixed-target Program (FXT) will extend collision energy range available for the analysis down to $\sqrt{s_{NN}} = 3.0$ GeV. BES-II along with FXT will dramatically enhance our understanding of the QCD phase diagram in the broad range of baryon chemical potential, μ_B, up to 720 MeV.

Recent detector upgrades increase STAR's acceptance both in rapidity and low transverse momentum, and extend its particle identification capabilities. With new detectors STAR can explore phase diagram with even higher precision hopefully reaching both the onset of deconfinement as well as the critical point.

In this talk, we present the most recent results and future plans from the STAR experiment.

PACS: 13.85.−t; 14.20.−c; 25.75.−q

[1] E-mail: aparin@jinr.ru

Strange hadron production

The main motivation for the Beam Energy Scan (BES) program at RHIC was to investigate properties of the Quantum ChromoDynamics (QCD) phase diagram in Au+Au collisions at different collision energies $\sqrt{s_{NN}} = 7.7 - 39$ GeV. First phase of BES took place in Run-10 and Run-11 with additional data taking in Run-14. Strange hadrons can be used to probe the phase boundary and onset of deconfinement. Strangeness enhancement in A+A with respect to p+p collisions has been suggested as a signature of phase transition to the state of quark-gluon plasma (QGP) [4]. The precise measurement of these yields in heavy ion collisions at BES energies may lead to a better understanding of strangeness production mechanisms in nuclear collisions and improve the extraction of the chemical freeze-out parameters.

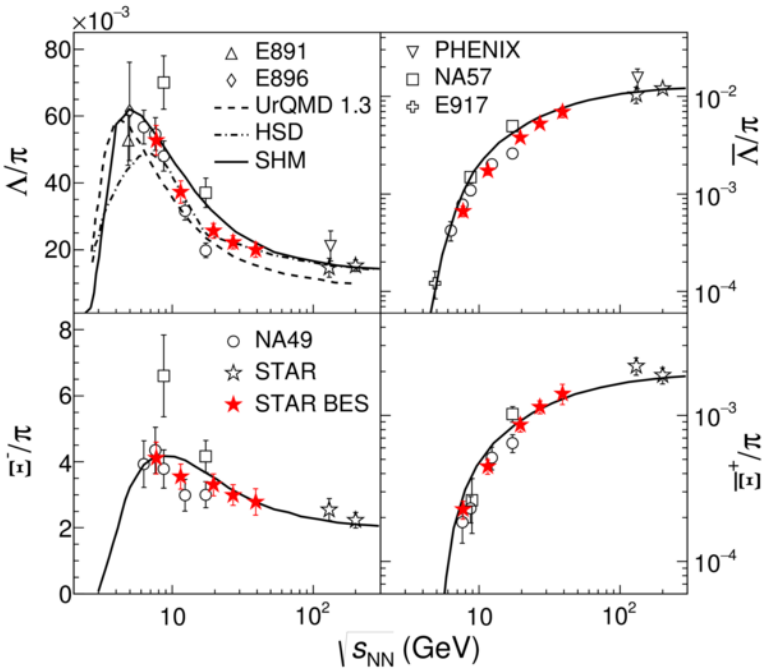

Fig. 1. Energy dependence of Λ, $\bar{\Lambda}$, Ξ^- and $\bar{\Xi}^+$ to pion, calculated as $1.5(\pi^- + \pi^+)$, ratios at mid-rapidity ($|y| < 0.5$) in central Au+Au collisions from STAR Beam Energy Scan phase I (solid symbols). Also plotted are existing results from AGS, SPS, PHENIX and STAR (open symbols) as well as calculations from hadronic transport models (UrQMD 1.3 and HSD) and a statistical hadron gas model (SHM) as dashed or solid lines. Plot is taken from [1].

We present STAR measurements of strange hadron (K^0_S, Λ, $\bar{\Lambda}$, Ξ^-, $\bar{\Xi}^+$, Ω^-, $\bar{\Omega}^+$ and ϕ) production at mid-rapidity $|y| < 0.5$ at five energies of BES-I. Transverse momentum spectra, averaged transverse mass, and the overall integrated yields of these strange hadrons were calculated versus the centrality and collision energy. Antibaryon-to-baryon ratio was used to test a thermal statistical model and to extract the temperature normalized strangeness and baryon chemical potentials at hadronic freeze-out (μ_B/T_{ch} and

μ_S/T_{ch}) in central collisions. It was compared to the previous results from NA49 and STAR experiments [1] - [3].

The p_T-integrated antibaryon-to-baryon ratios in central collisions were calculated for the STAR BES data and compared to those from STAR higher energies and NA49. It was found that the BES data are consistent with the NA49 data and fall within the published energy dependence trend. For all energies, the ratios show a hierarchy of $\bar{\Omega}^+/\Omega^- > \bar{\Xi}^+/\Xi^- > \bar{\Lambda}/\Lambda$ which is consistent with the predictions from statistical thermal models [5,6].

Figure 1 shows the ratios of Λ, $\bar{\Lambda}$, Ξ^-, $\bar{\Xi}^+$ yields at mid-rapidity to normalized yields of pions, i.e. $1.5(\pi^+ + \pi^-)$, in central Au+Au collisions obtained by STAR in BES-I in comparison with the calculations from hadronic transport models (UrQMD 1.3 and HSD) and a statistical hadron gas model (SHM). The Λ/π and Ξ^-/π ratios follow the trend previously observed in K^+/π^+ with a maximum around $\sqrt{s_{NN}} = 8$ GeV, which is consistent with the picture of maximum net-baryon density at freeze-out around this collision energy [7].

Figure 2 shows the nuclear modification factor, R_{CP} for K^0_S, $\Lambda + \bar{\Lambda}$, $\Xi^- + \bar{\Xi}^+$ ϕ, and $\Omega^- + \bar{\Omega}^+$ in Au+Au collisions at $\sqrt{s_{NN}} = 7.7 - 39$ GeV. R_{CP} is the ratio of particle yields in central collisions to those in peripheral ones scaled by the average number of inelastic binary collisions.

$$R_{CP} = \frac{[(dN/dp_T)/\langle N_{coll}\rangle]_{central}}{[(dN/dp_T)/\langle N_{coll}\rangle]_{peripheral}}$$

N_{coll} is determined from Glauber Monte Carlo simulations. If nucleus-nucleus collisions are just simple superposition of nucleon-nucleon collisions R_{CP} ratio will be equal to unity. Deviation of these ratios from unity suggests contributions from cold nuclear or in-medium effects. The energy evolution of strange hadron R_{CP} reflects the decreasing partonic effects with decreasing beam energies. In addition, the differences in R_{CP} for different particle species are apparent for $\sqrt{s_{NN}} > 19.6$. The differences become smaller at $\sqrt{s_{NN}} = 11.5$ GeV and eventually vanish at $\sqrt{s_{NN}} = 7.7$ GeV, which may suggest different properties of the system created in Au+Au collisions at lower collision energies.

Measurements of net-particle cumulants

Non-monotonic energy dependence of moments of the net-baryon or net-strangeness number distributions, related to the correlation length and the susceptibilities of the system, is suggested as an experimental signature for a critical point (CP) [8,9]. Current theoretical calculations are highly uncertain about the location of the CP. Numerical lattice QCD calculations at finite μ_B are limited by computing power. Upon approaching a critical point, the correlation length diverges and thus renders, to a large extent, microscopic details irrelevant. Hence observables like the moments of the conserved net-baryon or net-strangeness number distributions, which are sensitive to the correlation length, can be used in experimental search for a critical point. Higher moments of distributions of conserved quantities are more sensitive to the CP effects due to their stronger dependence on the correlation length. Cumulants of various orders were calculated to study the shape of the event-by-event net-particle distribution in detail, where

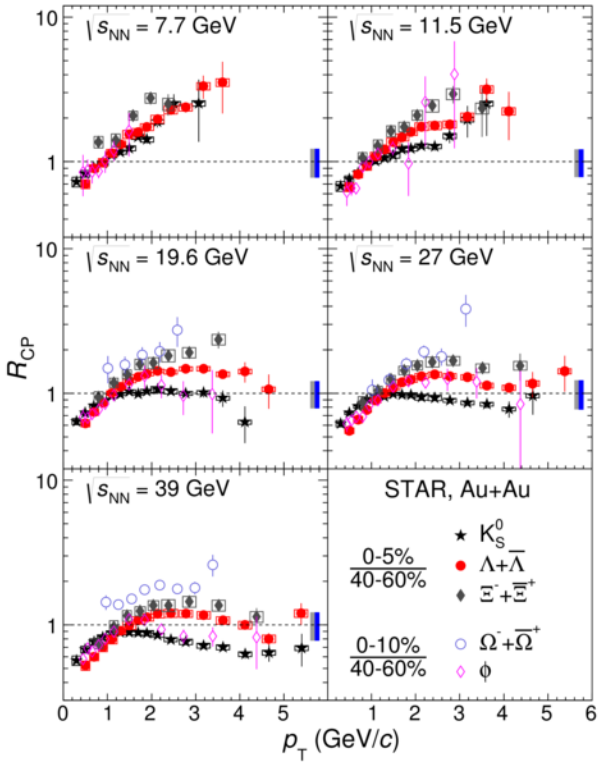

Fig. 2. $R_{CP}(0-5\%)/(40-60\%)$ for K^0_S, $\Lambda+\bar{\Lambda}$, $\Xi^- + \bar{\Xi}^+$ and $R_{CP}(0-10\%)/(40-60\%)$ for ϕ, $\Omega^- + \bar{\Omega}^+$ at mid-rapidity ($|y| < 0.5$) in Au+Au collisions at $\sqrt{s_{NN}} = 7.7 - 39$ GeV. The vertical bars denote the statistical errors. The box on each data point denotes the systematic uncertainty. There are only statistical errors for Ω and ϕ. The gray and blue bands on the right side of each panel represent the normalization errors from N_{coll} for $R_{CP}(0-5\%)/(40-60\%)$ and $R_{CP}(0-10\%)/(40-60\%)$ respectively. Plot is taken from [1].

$C_1 = M,\ C_2 = \sigma^2,\ C_3 = S\sigma^3,\ C_4 = \kappa\sigma^4$, with $M,\ \sigma,\ S,\ \kappa$ being mean, variance, skewness and kurtosis of the net-particle multiplicity distribution. Large values of C_3 and C_4 for central Au+Au collisions show that the distributions have non-Gaussian shapes, deviating from a Skellam expectation. This can be a first indication of enhanced fluctuations arising from a possible critical point. Ratios of cumulants are used in order to cancel volume variations to first order. Furthermore, these ratios of cumulants are related to the ratios of baryon-number susceptibilities $\chi^B_n = d^nP/d\mu^B_n$ at a given T and μ_B, as computed in QCD and QCD-based models, $C_3/C_2 = S\sigma = (\chi^B_3/T)/(\chi^B_2/T^2)$ and $C_4/C_2 = \kappa\sigma^2 = (\chi^B_4)/(\chi^B_2/T^2)$. Near the CP QCD-based calculations predict the non-Gaussian behavior of net-baryon number distributions and divergence of the susceptibilities, causing moments, especially higher-order quantities like $\kappa\sigma^2$, should have non-monotonic variation as a function of $\sqrt{s_{NN}}$.

Figure 3 shows the variation of C_3/C_2 and C_4/C_2 for net-proton multiplicity distributions as a function of $\sqrt{s_{NN}}$ for central and peripheral Au+Au collisions in the energy

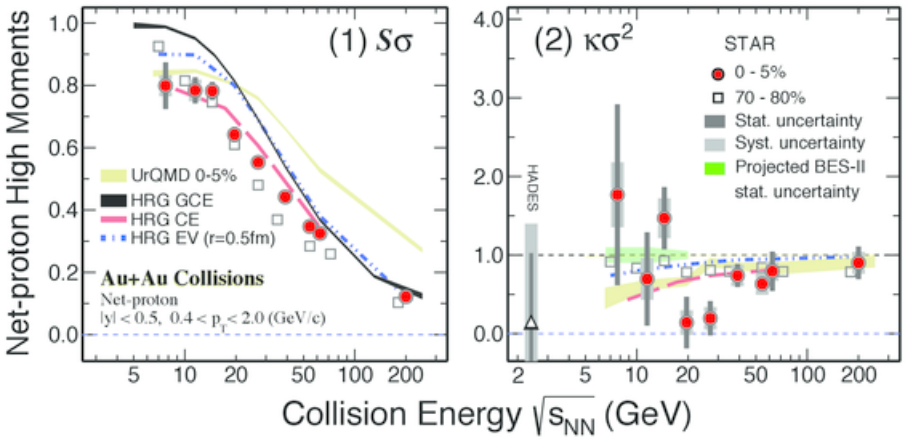

Fig. 3. Measured values of $S\sigma$ (1) and $\kappa\sigma^2$ (2) as a function of collision energy for net-proton distributions measured in Au+Au collisions. The results are shown for central $0-5\%$ (filled circles) and peripheral $70-80\%$ (open squares) collisions within $0.4 < p_T(GeV/c) < 2.0$ and $|y| < 0.5$. The vertical narrow and wide bars represent the statistical and systematic uncertainties, respectively. It is compared with hadron resonance gas and UrQMD model calculations for central $0-5\%$ collisions [11].

range $\sqrt{s_{NN}} = 7.7-62.4$ GeV. In central collisions a non-monotonic variation with beam energy is observed for $\kappa\sigma^2$. This ratio goes below unity (statistical baseline) and then rises towards values above unity with decreasing beam energy. The peripheral collisions on the other hand show a monotonic variation with $\sqrt{s_{NN}}$ and $\kappa\sigma^2$ values are always below unity. The deviation of the measured $\kappa\sigma^2$ from several baseline calculations with no critical point, and its non-monotonic dependence on $\sqrt{s_{NN}}$, are qualitatively consistent with the expectations from QCD-based models including a critical point.

Net-kaons and net-protons have been used as proxies for the net-strangeness [10] and net-baryon number [11], respectively. STAR presented the measurement of efficiency and centrality bin width corrected cumulant ratios $(C_2/C_1, C_3/C_2)$ of net-Λ distributions, which has both strangeness and baryon number conservation, as a function of collision energy, centrality and rapidity for Au+Au collisions at five beam energies $\sqrt{s_{NN}} = 19.6, 27, 39, 62.4$ and 200 GeV. The ratios of the measured cumulants show no features of critical fluctuations [12].

The volume independent cumulant ratios, $C_2/C_1 = \sigma^2/M$ and $C_3/C_2 = S\sigma$, of net-Λ distributions were measured as a function of collision centrality in Au+Au collisions in energy range $\sqrt{s_{NN}} = 19.6-200$ GeV. C_2/C_1 demonstrates no significant dependence of the collision centrality due to the volume independence of the cumulant ratios, while it increases as a function of increasing collision energy for a given centrality class, which is dominated by the energy dependence of C_1. The net-Λ C_3/C_2 measurement shows only a weak dependence on the collision centrality. It decreases as a function of increasing collision energy mainly due to the energy dependence of the net-Λ C_3.

Figure 4 shows the comparison of measured ratios obtained for net-Λ, net-kaons [10] and net-protons in most central collisions [11]. The net-Λ data follow more closely the net-

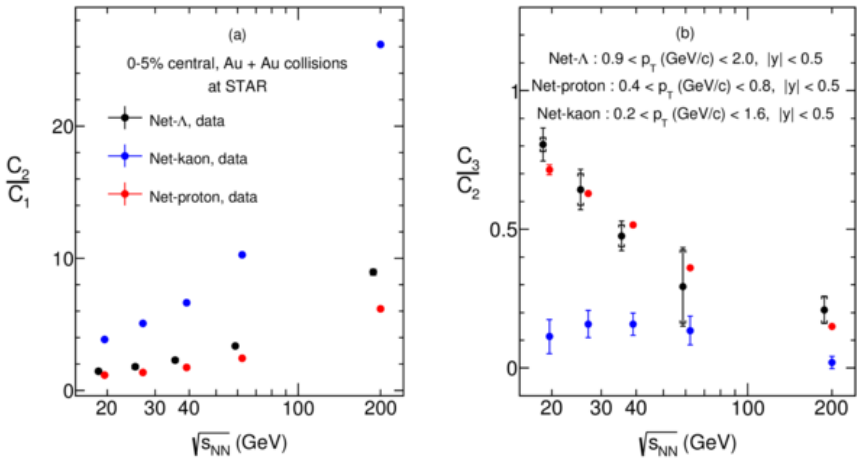

Fig. 4. Beam energy dependence of net-Λ (in black), net-proton (in red) and net-kaon (in blue) cumulant ratios, (a) C_2/C_1 and (b) C_3/C_2, in most central $(0-5\%)$ Au+Au collisions. The vertical lines represent the statistical uncertainties and caps represent systematic uncertainties. The black data points are shifted to the left for clarity.

proton data, which can be expected since the abundance and imbalance between particle and anti-particle for the Λ baryon is more closely aligned with the proton numbers than with the mesonic strange state [7].

Hypertriton measurements

CPT theorem states that the combined operation of charge conjugation, parity transformation and time reversal must be conserved. This requires particles and corresponding antiparticles to have the same mass and lifetime but opposite charge and magnetic moment. STAR has performed the first precise test of the CPT symmetry in a nucleus containing a strange quark, the hypertriton. This hypernucleus is the lightest one yet discovered and consists of a proton, a neutron and a Λ hyperon. Experimental data in this measurements were recorded during Run-14 and Run-16 in Au+Au collisions at $\sqrt{s_{NN}} = 200$ GeV [13,14]. STAR has measured the Λ hyperon binding energy B_Λ within the hypertriton, and has found that it differs from the widely used value [15] and from predictions [16], where the hypertriton is treated as a weakly bound system. Hypernuclei are natural hyperon–baryon correlation systems, thus providing direct access to the hyperon–nucleon interaction through measurements of the binding energy B_Λ in a hypernucleus.

The hypertriton candidates were reconstructed from the invariant mass distributions of the daughters: ${}^3He + \pi^-$ for the 2-body, and $d + p + \pi^-$ for the 3-body decay channel of ${}^3_\Lambda H$ and ${}^3\bar{H}e + \pi^+$ for the 2-body, and $\bar{d} + \bar{p} + \pi^+$ for the 3-body decay channel for ${}^3_\Lambda\bar{H}$.

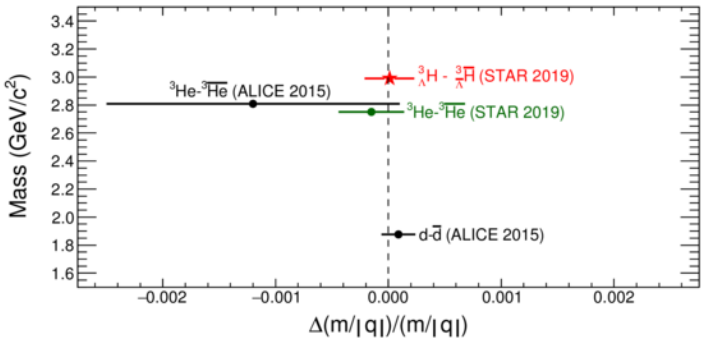

Fig. 5. Measurements of the relative mass-to-charge ratio differences between different nuclei and antinuclei species. The current measurement of the relative mass difference $\Delta m/m$ between ${}^{3}_{\Lambda}H$ and ${}^{3}_{\bar{\Lambda}}\bar{H}$ constrained by the existing experimental limits for decay daughters is shown by the red star marker. The green point is the new ^{3}He result after applying the constraint provided by the present ${}^{3}_{\Lambda}H$ result. The differences between d and $\bar{d}$ and between ^{3}He and anti-^{3}He measured by the ALICE Collaboration are also shown. The two ^{3}He and anti-^{3}He points are staggered vertically for visibility. The dashed vertical line at zero is the expectation from CPT invariance. The horizontal error bars represent the sum in quadrature of statistical and systematic uncertainties. Plot is taken from [17].

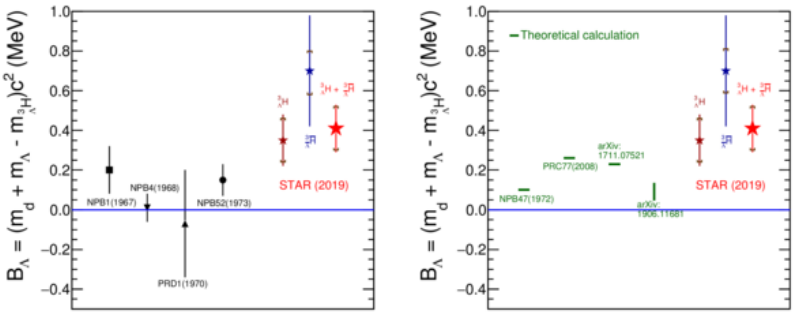

Fig. 6. Measured values of Λ binding energy in hypertriton and anti-hypertriton compared with previous results and theoretical predictions. The black points and their error bars (which are the reported statistical uncertainties) represent for ${}^{3}_{\Lambda}H$ based on earlier data. The current STAR measurement plotted here is based on a combination of ${}^{3}_{\Lambda}H$ and ${}^{3}_{\bar{\Lambda}}\bar{H}$ assuming CPT invariance. Error bars show statistical uncertainties and caps show systematic errors. The green solid lines in the right panel represent theoretical calculations. The horizontal blue lines in both panels indicate a reference energy corresponding to zero binding of the Λ hyperon. Plot is taken from [17].

Recunstructed invariant mass for ${}^{3}_{\Lambda}H$ is 2990.95 $\pm$ 0.13 (*stat.*) $\pm$ 0.11 (*syst.*) MeV/c^2, for ${}^{3}_{\Lambda}\bar{H}$ is 2990.60 $\pm$ 0.28 (*stat.*) $\pm$ 0.11 (*syst.*) MeV/c^2, giving the combined hypertriton mass m = 2990.89 $\pm$ 0.12 (*stat.*) $\pm$ 0.11 (*syst.*) MeV/c^2. Figure 5 demonstrates the mass-to-charge ratio differences measured by STAR and ALICE experiments [17, 18]. Combined data from 2- and 3-body decays give the result on mass difference:

$$\frac{\Delta m}{m} = \frac{m_{^3_\Lambda H} - m_{^3_{\bar{\Lambda}}\bar{H}}}{m} = (0.1 \pm 2.0\ (stat.)\ \pm\ 1.0\ (syst.)) \times 10^{-4}$$

The Λ binding energy of ${}^3_\Lambda H$ is defined as $B_\Lambda = m_d + m_\Lambda - m_{^3_\Lambda H}$, where m_d, m_Λ and $m_{^3_\Lambda H}$ are the deuteron mass, the Λ hyperon mass and the mass of ${}^3_\Lambda H$, respectively. It was calculated that $B_\Lambda = 0.41 \pm 0.12\ (stat.)\ \pm\ 0.11\ (syst.)$ MeV. This binding energy is presented in Fig. 6 compared with other experimental measurements and theoretical calculations. The obtained result differs from zero with a statistical significance of 3.4σ, and the central value of the current STAR measurement is larger than the commonly used value [15].

Dielectron production

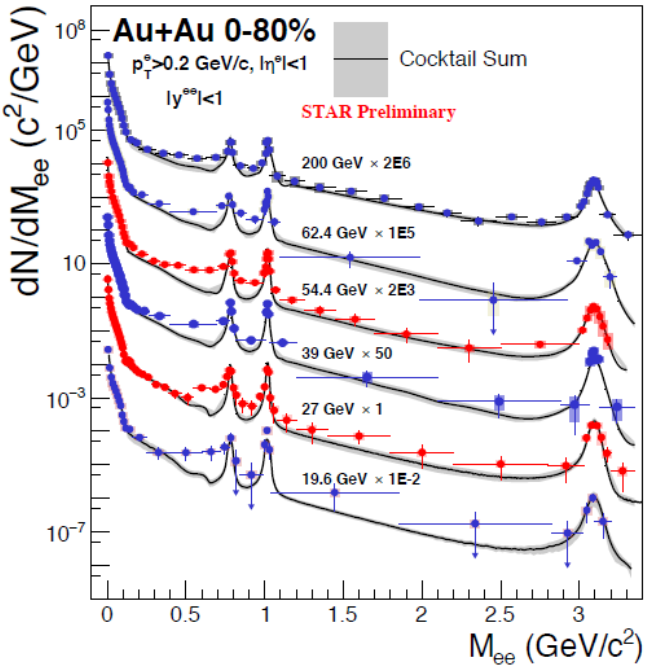

Fig. 7. Background subtracted dielectron invariant mass spectra within the STAR acceptance for 0−80% most central Au+Au collisions at $\sqrt{s_{NN}} = 19.6, 27, 39, 54.4, 62.4$ and 200 GeV. Error bars and open boxes represent the statistical and systematic uncertainties in the measurements. The black solid curves represent the hadronic cocktail with the gray bands representing the cocktail uncertainties.

Dileptons are good probes of the hot QCD matter created in heavy-ion collisions because leptons are not affected by the strong interaction. This allows leptons to traverse the hot medium with minimal final-state effects and provide an experimental test to the predicted chiral symmetry restoration. Figure 7 presents systematic measurements of dielectron invariant mass M_{ee} spectra at mid-rapidity $|y^{ee}| < 1$ in Au+Au collisions at $\sqrt{s_{NN}} = 27, 39, 54.4$ and 62.4 GeV [19] - [21]. Accumulated datasets cover an order-of-magnitude range in collision energies where the total baryon density and freeze-out temperatures stay remarkably constant. For all energies studied, a significant excess yield of dielectrons is observed in the low-mass region ($0.40 < M_{ee} < 0.75$ MeV/c^2) compared to hadronic cocktail simulations at freeze-out. The normalized excess yields in the low-mass region show no significant collision energy dependence. The reason for such a behavior may be because dilepton production in the medium is expected to be mainly determined by the strong coupling of the ρ meson to baryons, rather than to mesons [22]. This is well described by several models which include an in-medium broadening of the ρ meson spectral function.

Future results from BES-II which has over order-of-magnitude more data in low collision energy region may allow us to better understand the competing factors that play a role in the low-mass region dielectron excess production and to further clarify the connection between ρ meson broadening and chiral symmetry restoration.

Jet measurements

Figure 8 shows the nuclear modification factor $R_{CP} = (0-10\%)/(60-80\%)$ of charged jets as a function of jet transverse momentum p_T for jet radius $R = 0.3$ in Au+Au collisions at $\sqrt{s_{NN}} = 200$ GeV [23]. The measured R_{CP} shows no clear $p_{T,jet}$ dependence at RHIC within the uncertainties. The R_{CP} magnitude measured at RHIC is close to the one measured at LHC [24] although they are measured at different $p_{T,jet}$ intervals. It is also compared with R_{CP} of charged hadron measured at RHIC [25] and LHC [26], and they are consistent in the overlapping p_T regions. The significant rising trend of the charged hadron R_{CP} at high p_T is not observed in the charged jet R_{CP}. The correlation between the hadron p_T and its parent jet p_T reflects the fragmentation process, which may result in a different p_T dependence of R_{CP} for the charged hadrons and jets. New measurements with better precision are necessary to provide more stringent constraints on the mechanism of jet quenching.

Summary

STAR experiment presented a set of recent results on heavy ion physics. Precise measurements of strange hadron production at low energies $\sqrt{s_{NN}} = 7.7-39$ GeV are consistent with previous observation as well as with theory expectations. It suggests a change of the hadron production mechanism at energy $\sqrt{s_{NN}} \approx 8$ GeV. The fluctuations of conserved quantum numbers such as net-charge, net-baryon number and net-strangeness provide useful information about the nuclear matter phase transition. The measured cumulant ratios of net-charge, net-proton and net-kaon multiplicity distributions obtained

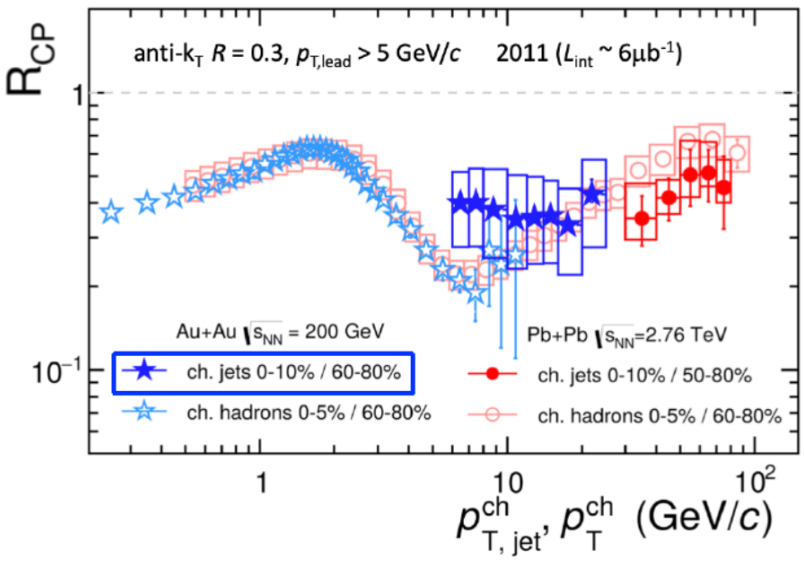

Fig. 8. First measurement of charged jet nuclear modification factor R_{CP} (solid blue stars) for jet radius $R = 0.3$ in Au+Au collisions at $\sqrt{s_{NN}} = 200$ GeV. It is compared to results from LHC Pb+Pb collisions at $\sqrt{s_{NN}} = 2.76$ TeV (solid red dots), as well as charged hadron R_{CP} from STAR (open blue stars) and LHC (open red dots). The vertical bars (boxes) denote the statistical (systematic) uncertainties. Plot is taken from [23]

in Au+Au collisions at collision energy range $\sqrt{s_{NN}} = 7.7 - 200$ GeV at STAR have been compared to UrQMD and HRG calculations in a search for the critical point. STAR has presented the first measurement of CPT invariance in the sector of hypernuclear matter where (anti-) strange quarks play a role in (anti-) nuclear binding. The relative mass difference between the hypertriton and antihypertriton is found consistent with no violation of CPT symmetry. We reported a new measurement of the Λ hyperon binding energy in the hypertriton. The value differs from zero with a significance of 2.6σ and is larger than the prior measurement which is widely used. These results constrain the hyperon-nucleon interaction, providing improved data to understand the role of hyperons in neutron stars. Dielectron yield measurements at 27 and 54.4 GeV confirm an excess previously observed at low-mass region ($0.40 < M_{ee} < 0.75$ MeV/c^2) at mid-rapidity $|y^{ee}| < 1$ and $p_T^e > 0.2$ GeV/c. First measurement of charged jet nuclear modification factor R_{CP} obtained at STAR in Au+Au collisions at $\sqrt{s_{NN}} = 200$ GeV was presented and compared with jet results at ALICE in Pb+Pb collisions at $\sqrt{s_{NN}} = 2.76$ TeV and charged hadron R_{CP} from STAR and LHC. Comparison of the results may suggest a different p_T dependence of R_{CP} for charged hadrons and jets.

REFERENCES

1. *J. Adam et al.* [STAR collaboration], Phys. Rev. C — 2020. — V. 102. — P. 34909.
2. *C. Alt et al.* [NA49 Collaboration], Phys. Rev. Lett. — 2005. — V. 94. — P. 192301.
3. *C. Alt et al.* [NA49 Collaboration], Phys. Rev. C — 2008. — V. 77. — P. 024903.
4. *J. Rafelski and B. Muller*, Phys. Rev. Lett. — 1982. — V. 48. — P. 1066.
5. *F. Becattini, J. Cleymans, A. Keranen, E. Suhonen and K. Redlich*, Phys. Rev. C — 2001. — V. 64. — P. 024901.
6. *A. Andronic, P. Braun-Munzinger and J. Stachel*, Nucl. Phys. A — 2006. — V. 772. — P. 167.
7. *L. Adamczyk et al.* [STAR collaboration], Phys. Rev. C — 2017. — V. 96. — P. 044904.
8. *Stephanov, M.A., Rajagopal, K., and Shuryak, E.V.*, Phys. Rev. D — 1999. — V. 60. — P. 114028.
9. *Gavai, R.V., and Gupta, S.*, Phys. Lett. B — 2011. — V. 696. — P. 459.
10. *J. Adam et al.* [STAR collaboration], Phys. Lett. B — 2018. — V. 785. — P. 551.
11. *J. Adam et al.* [STAR collaboration], arXiv:2001.02852v2
12. *J. Adam et al.* [STAR collaboration], Phys. Rev. C — 2020. — V. 102. — P. 24903.
13. *Contin, G., Greiner L., Schambach J., Szelezniak M., Anderssen E. et al.* Phys. Res. A — 2018. — V. 907. — P. 60–80.
14. *Llope, W. J. et al.* [STAR collaboration], Nucl. Inst. Methods Phys. Res. A — 2012. — V. 661. — P. 110–113.
15. *Juric, M., Bohm G., Klabuhn J., Krecker U., Wysotzki F. et al.* Nucl. Phys. B — 1973. — V. 52. — P. 1-30.
16. *Haidenbauer, J., Meiβner, U.-G., Nogga, A.* arXiv:1906.11681.
17. *J. Adam et al.* [STAR collaboration], Nature Physics — 2020. — V. 16. — P. 409.
18. *J. Adam, et al.* [ALICE Collaboration], Nature Physics— 2015. — V. 11. — P. 811.
19. *L. Adamczyk et al.* [STAR collaboration], arXiv:1810.10159 [nucl-ex].
20. *L. Adamczyk et al.* [STAR collaboration], Phys. Rev. C— 2015. — V. 92. — P. 024912.
21. *L. Adamczyk et al.* [STAR collaboration], Phys. Lett. B— 2015. — V. 750. — P. 64.
22. *R. Rapp, J. Wambach, and H. van Hees*, Relativistic Heavy Ion Physics, edited by R. Stock (Springer-Verlag, 2010), vol. 23 of Group I: Elementary Particles, Nuclei and Atoms, chap. 4, pp. 1–42.
23. *J. Adam et al.* [STAR collaboration], — arXiv:2006.00582 [nucl-ex].

24. *B. Abelev et al.* [ALICE collaboration], — JHEP — 2014. — V. 03. — P. 013. — arXiv:1311.0633 [nucl-ex].

25. *J. Adam et al.* [STAR collaboration], — Phys. Rev. Lett. — 2003. — V. 91. — P. 172302. — arXiv:0305015 [nucl-ex].

26. *G. Aad et al.* [ATLAS collaboration], JHEP — 2015. — V. 09. — P. 050. — arXiv:1504.04337 [hep-ex].